DOI: 10.1002/cmdc.200700197

Fragmental Modeling of Human Glutamate Transporter EAAT1 and Analysis of its Binding Modes by Docking and Pharmacophore Mapping

Alessandro Pedretti,[a] Laura De Luca,[b] Cristina Sciarrillo,[a] and Giulio Vistoli*[a]

The objective of the study was to generate a reliable model of the homotrimeric structure for the human glutamate transporter EAAT1, based on experimental folding of transporter homologue from Pyrococcus horikoshii. The monomer structure was derived using a fragmental approach and the homotrimer was assembled using protein–protein docking. The interaction capacities of the EAAT1 model were explored by docking a set of 32 known ligands including both substrates and blockers. Docking results unveiled that the substrates' bioactivity is strongly influenced by a precise fitting between the ligand and the EAAT1 binding site, wheras the blockers' activity depends on a set of apolar contacts that ligands can realize in an adjacent hydrophobic subpocket. The docking results were further verified by generating two pharmacophore models (the first for substrates and the latter for blockers) which revealed the features necessary for high EAAT1 activity. The consistency of docking results and the agreement with pharmacophore models afford an encouraging validation for the EAAT1 model and emphasize the soundness of the fragmental approach to model any transmembrane protein.

Introduction

The amino acid L-glutamate represents the main excitatory neurotransmitter in the mammalian CNS where it activates a broad assortment of ionotropic and metabotropic receptors and mediates various forms of neuronal communications including development and plasticity, learning and memory, cognition, pain, and nociception.[1,2] The physiological roles of L-glutamate are counteracted by its ability to overactivate the ionotropic receptors triggering a series of destructive processes which induce neuronal death.[3] Such glutamate-mediated neuronal damage is involved in both acute and chronic neurological diseases, including amyotrophic lateral sclerosis (ALS), Alzheimer's disease, epilepsy, and CNS ischemia.[4] Hence, the amount of extracellular L-glutamate must be finely regulated to assure critical signalling yet avoiding excitotoxic phenomena. In this context, the L-glutamate transporters (excitatory amino acid transporters, EAATs) have attracted remarkable attention, also because the glutamate system is lacking in an extracellular enzyme which rapidly degrades the neurotransmitter.[5–8]

On these grounds, several EAAT ligands have been studied in the last few years as novel therapeutics against neurodegenerative diseases.[9–11] Overall, the EAAT ligands can be classified as natural substrates, substrate inhibitors, and nontransported uptake blockers.[12] The interest in designing EAAT inhibitors (both substrates and blockers) resides in the observation that in pathological conditions, when the electrochemical gradient is damaged, EAATs can operate in a reverse mode, thus overactivating post-synaptic receptors.[13,14]

Molecular cloning and molecular biological studies have identified five human EAAT subtypes (EAAT1-5), possessing distinct cellular localization, modulation, mechanism, and pharmacological profile.[15] EAAT1–4 are present in the mammalian CNS, whereas EAAT5 is located exclusively in the retina, largely acting as a chloride channel.[16] All subtypes belong to the class of Na^+ dependent transporters and are electrogenic as two net positive charges are moved into the cell for each transport cycle.[17] The present study is focused on the EAAT1 subtype, which is the human homologue of the rodent GLAST (glutamate–aspartate transporter). It is predominantly located in the cerebellar Bergmann glia, but it is also present in glial cells throughout the CNS, and in a small number of neurons.[18] It is also expressed in some peripheral organs and tissues (for example, in the retina Muller cells[16]).

EAATs have a homotrimeric architecture[19] in which each monomer is characterized by a single amino acidic chain (rang-

[a] *A. Pedretti, C. Sciarrillo, G. Vistoli*
Istituto di Chimica Farmaceutica e Tossicologica "Pietro Pratesi", Facoltà di Farmacia, Università degli Studi di Milano, Via Mangiagalli, 25, I-20133 Milano (Italia)
Fax: (+39) 02-50319359
E-mail: giulio.vistoli@unimi.it

[b] *L. De Luca*
Dipartimento Farmaco-Chimico, Facoltà di Farmacia, Università di Messina, Viale Annunziata, I-98168 Messina (Italia)

Supporting information for this article is available on the WWW under http://www.chemmedchem.org or from the author.

ing from 500 to 600 residues) including eight transmembrane helices (TM1–8) and two transmembrane helical hairpins (HP1–2). The transmembrane segments are connected by five extracellular loops (EL1–5) and four cytoplasmic loops (CL1–4). Interestingly, both terminal segments (N-T and C-T) are located in the intracellular side.[20]

Mutational analyses have allowed the identification of some key residues involved in substrate recognition.[21] Concerning the EAAT1 subtype, Arg 479 (TM8) contacts the glutamate γ-carboxyl group and sequentially binds glutamate and potassium enabling the coupling of their fluxes.[22] The residues between Pro 392 and Gln 415 (TM7) belong to a highly conserved re-entrant membrane loop at the cell surface and may include part of the translocation pore for substrates and cotransported ions.[23] Finally, the mutation of Val 449 (HP2) eliminates substrate transport but not the substrate-gated anion conductance.[24]

As EAATs are transmembrane proteins, their structure cannot be easily resolved and this can hamper the rational design of novel ligands. Fortunately, the prediction of the EAAT folding can be supported by the recent resolution of the glutamate transporter homologue from *Pyrococcus horikoshii* which revealed the EAAT topology providing an atomic description for the mechanism of substrate and ion transport.[25] Hence, we undertook to generate, firstly, a three-dimensional model of full-length human EAAT1 monomer by homology modelling, and then the corresponding homotrimer through protein–protein docking. Although it was possible to model the human EAAT1 monomer using the resolved glutamate transporter homologue as an unique template,[26] we preferred to exploit a fragmental approach for two main reasons: 1) three significant EAAT1 segments were yet unpredictable using the glutamate transporter homologue as the template (as detailed in the Methods section); 2) the fragmental strategy allows exploration of the local features of human EAAT1, avoiding a model which loses its structural peculiarities by being forced to comply with the structure of the glutamate transporter homologue. Interestingly, such a fragmental approach reflects a more general trend in folding prediction which favors local homology combining more predictive algorithms (the so-called meta-prediction).[27]

The fragmental approach has been recently developed by us to generate a reliable model of human ghrelin receptor (hGHS-R1a) in the open[28] and closed state[29] and the present study was also designed to verify the soundness of such an approach by modeling a totally different transmembrane protein. Firstly, the model "goodness" was checked by docking a series of EAAT1 ligands, taken from literature, including both substrates (Figure 1) and blockers (Figure 2). Then, two pharmacophore models, the first for substrates and the latter for blockers, were built with the aim of confirming the docking analyses rationalizing the key features required for an optimal EAAT1 activity and revealing the binding details able to discriminate among substrates and blockers.

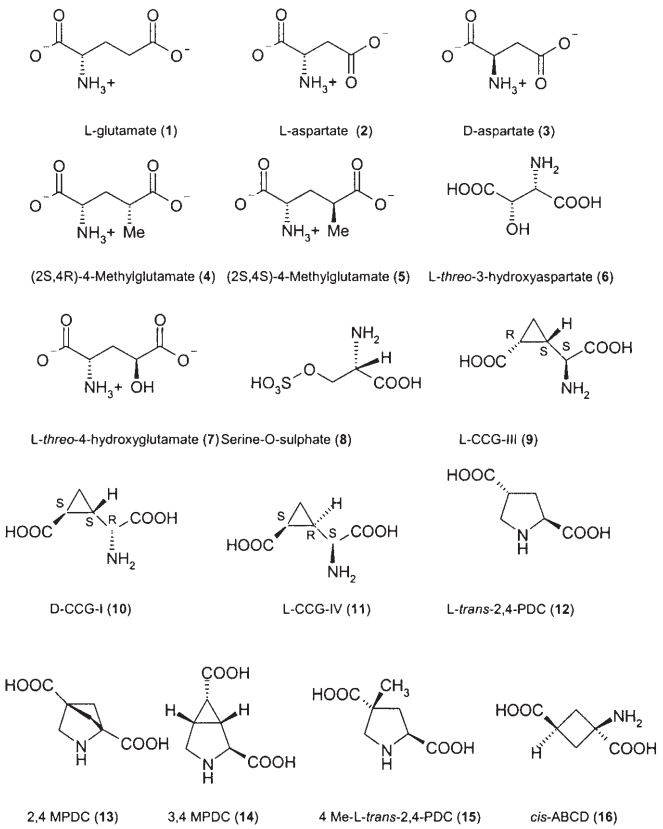

Figure 1. Natural substrates (**1**–**3**) and substrate inhibitors (**4**–**16**).

Results and Discussion

EAAT1 monomer structure

Figure 3 presents the tube structure of the EAAT1 monomer, showing the typical topology of Na^+ dependent transporters with eight transmembrane helices (TM1–8) and two transmembrane helical hairpins (HP1–2). Overall, the EAAT1 monomer has a truncated conic shape, where the intracellular side is wider than the extracellular one, mainly because of the presence in the cytoplasm of both terminal domains. The N-terminal domain (N-T) domain is rich in cationic residues which anchor the protein to phospholipidic heads and constrain its hairpin conformation, mainly stabilized by H-bonds plus some pivotal ionic bridges.

Apart from TM4 and TM7, the transmembrane segments show a regular α-helical folding, as already observed in the transmembrane segments of GPCRs, even if they are characterized by an unusual length for such segments (for example, TM3, TM5, and TM8 have more than 30 residues). Conversely, TM4 and TM7 are composed by multiple elements with an uncommon folding which deserves a detailed description. Thus, TM4 is formed by three separated and nearly parallel α-helices (namely TM4a, TM4b, and TM4c) connected by two interhelical loops (L4ab and L4bc). The former is a very short bridge which acts as a spacer as the axes of TM4a and TM4b remain almost parallel but distanced by about 8 Å. The latter is a long loop which characterizes the human EAAT1 structure as it is absent in the glutamate transporter homologue from *Pyrococcus hori-*

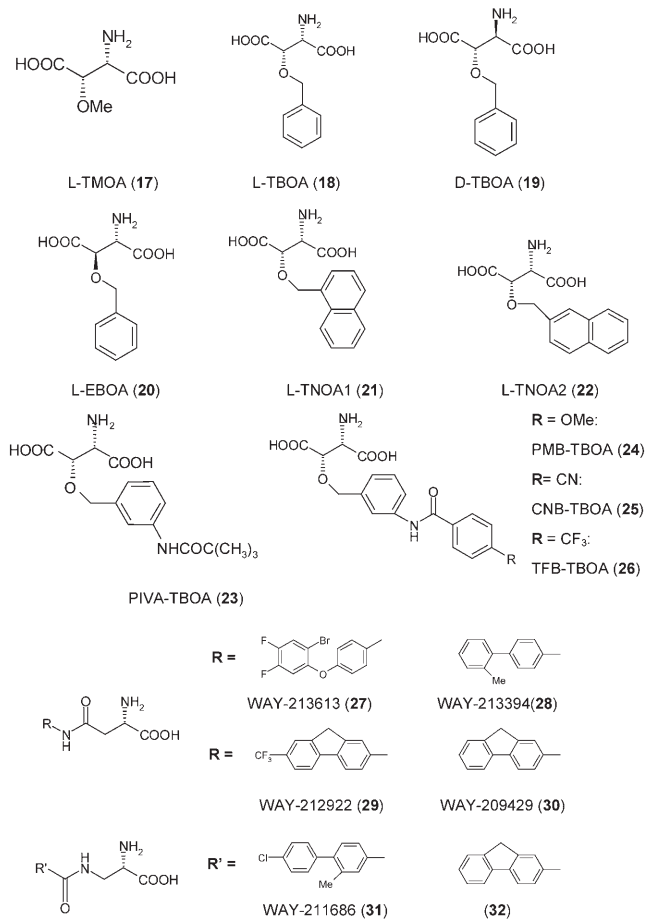

Figure 2. Nontransported blockers (**17**–**32**).

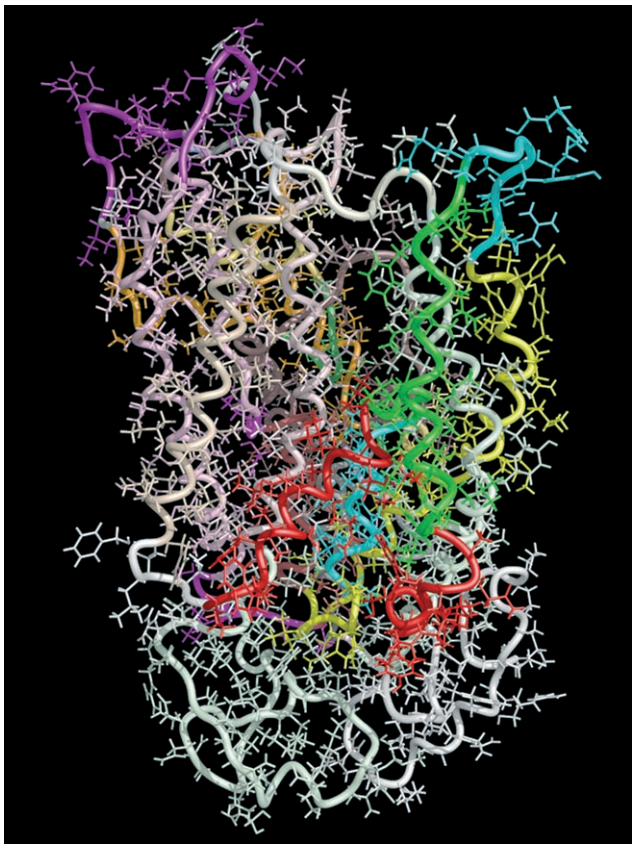

Figure 3. Tube structure of EAAT1 monomer model coloured by segment.

koshii. This loop shows an ellipsoidal shape being placed almost perpendicularly to TM4b and TM4c helices. It shows a central helical motif (Glu 207–Arg 226) surrounded by two hairpins (Phe 190–Asn 206 and Ile 227–Leu 244) to which TM4b and TM4c are connected. Noticeably, the second loop, despite being markedly more complex, has the same spacer effect of L4ab, as TM4b and TM4c conserve their axes nearly parallel and distanced by about 10 Å. Finally, TM7 has a folding very similar to that of the TM4a-L4ab-TM4b segment, formed by two parallel helices connected by a short extended bridge.

The transmembrane bundle of human EAAT1 monomer also comprises two helical hairpins (that is, HP1–2) characterized by helix-turn-helix motifs. Specifically, HP1 is placed between TM6 and TM7 beginning in the cytoplasm and inserting into the membrane, whereas HP2 is interposed between TM7 and TM8 and is largely exposed in the extracellular basin. The turn of HP1 domain includes a serine-rich segment which seems crucial for the glutamate transporter,[30] whereas the HP2 turn is constrained by a central conserved proline.

Taken globally, the transmembrane bundle is composed by a distorted cylinder whose surface is lined by TM1–6 segments, whereas TM7–8 helices and helical hairpins form the transmembrane core implicated in substrate transport. The interhelix distances (as compiled in Table S1, Supporting Information) help to clarify the precise organization of the transmembrane bundle showing that the arrangement of TM1–6 segments does not agree with the numerical order, as TM5 is inserted between TM1 and TM2, TM4 is inserted between TM2 and TM3, and finally TM6 closes the crown connecting TM3 with TM1. The distance averages also confirm that HP1, HP2, TM7, and TM8 form the core of transmembrane bundle. Specifically, TM7 and TM8 take a central position spanning the entire membrane and surrounded by the helical hairpins (HP1 towards the cytoplasm and HP2 towards the extracellular side). Both hairpin domains penetrate into the membrane even if the greater interhelix distance average of HP2 confirms that this hairpin is less buried being almost parallel to membrane plane. The described arrangement of helical hairpins seems to confirm that they could act as internal (HP1) and external (HP2) gates modulating transport.[31]

Whereas the external crown (that is, TM1–6) is stabilized by hydrophobic contacts and the polar interactions are rare, in the central core (that is, TM7–8, HP1–2) the polar interactions are more abundant both between transmembrane helices and between helices and hairpins also because TM8 has an amphipathic character with one face lining the aqueous pathway.[32] The intracellular loops (CL1-4) are very short segments which assume turn motifs largely stabilized by H-bonds and ionic contacts. Due to their shortness, they neither penetrate the transmembrane segment nor interact between them. On the other hand, the extracellular loops (EL1–5) are usually longer and assume more complex conformations, as in the case of

EL2 which shows an uncommon extended arch-shape folding. Also the extracellular loops do not insert in the membrane and are too far to stabilize interactions between them. Finally, the C-terminal domain (C-T) is rich in hydrophilic residues and shows strand motifs strongly stabilized by polar interactions.

EAAT1 homotrimeric architecture

Figure 4A and B illustrate the tube structure of the EAAT1 homotrimer showing its global bowl shape with a threefold symmetry axis perpendicular to the membrane. In particular, Figure 4A shows the trimer viewed from the cytoplasmic side unveiling the central basin and the global triangular shape with a size of about 90 Å. Viewed parallel to the membrane (Figure 4B), the trimer is about 80 Å in height. The transmembrane portion lies approximately in the middle, thus suggesting that the EAAT1 trimer protrudes about 20 Å from each side of membrane bilayer.

To determine which segments are mainly involved in intersubunit interfaces, the accessible surface values of each segment in the three monomers were calculated and compared with the corresponding SAS values in the EAAT1 monomer alone (as compiled in Table S2, Supporting Information). The segments which show the most significant SAS differences are TM2, TM4, and TM8. In particular, TM2, TM4, and, less so, TM5 and TM1 are involved in intersubunit interface stabilization, whereas the amphipathic TM8 segment lines the central aqueous basin. A visual scrutiny of trimer structure unveils that TM4 takes a pivotal position interacting with TM1, TM2, and TM5 of neighboring subunits. The intersubunit contacts are more abundant in the cytoplasmic side, where the trimer shows a pointed surface, than in the extracellular one.

Figure 4C depicts the "DEEP" surface of EAAT1 trimer, calculated by VEGA software (as explained in the Methods section), which reveals the geometric features of pockets and crevices. In particular, Figure 4C clearly shows the central basin which is as large as 50 Å in diameter and 30 Å in depth. As the basin dips into the membrane plane and its surface is hydrophilic, the aqueous solution reaches the midpoint of the membrane bilayer. The intersubunit surfaces define three crevices lined by TM1, TM4, and TM6. These crevices allow lipid molecules to contact helical hairpins, providing a structural basis for understanding how lipids can modulate the EAAT1 activity.

Docking results: Natural substrates

Figure 5A shows the main interactions stabilizing the complex between L-glutamate (**1**) and EAAT1. As revealed by mutational studies, the ligand's γ-carboxylate forms an ion-pair with Arg 479 (TM8). Other key interactions involve the ligand ammonium group which forms H-bonds with the side chains of Gln 204 (TM4), Gln 445 (HP2), and Thr 450 (HP2), and the α-carboxylate which establishes H-bonds with the backbone of Val 449 (HP2), Met 451 (HP2), and with the side chain of Thr 450. Finally, the apolar side chain of Met 451 lines the glutamate carbon skeleton. Despite the narrowness of the binding site and the precise topography of the revealed interactions, the large extent of the positive charge of Arg 479 guanidine group allows stabilization of the salt bridge with γ-carboxylate even preserving significant mobility of the glutamate χ_2 torsion which can assume both antiperiplanal (extended glutamate conformers as seen in Figure 5A) and synclinal geometries (folded glutamate conformers, complexes not shown), showing in all cases a nearly identical pattern of stabilizing interactions. Such a conformational freedom suggests that the distance between ligand carboxylates should not be a critical factor in determining the bioactivity as demonstrated by its marked variability among the docked ligands (as compiled in Table 1). Conversely, the region which interacts with the ligand ammonium and α-carboxylate appears vastly more constrained possibly because of the greater number of implicated residues and the

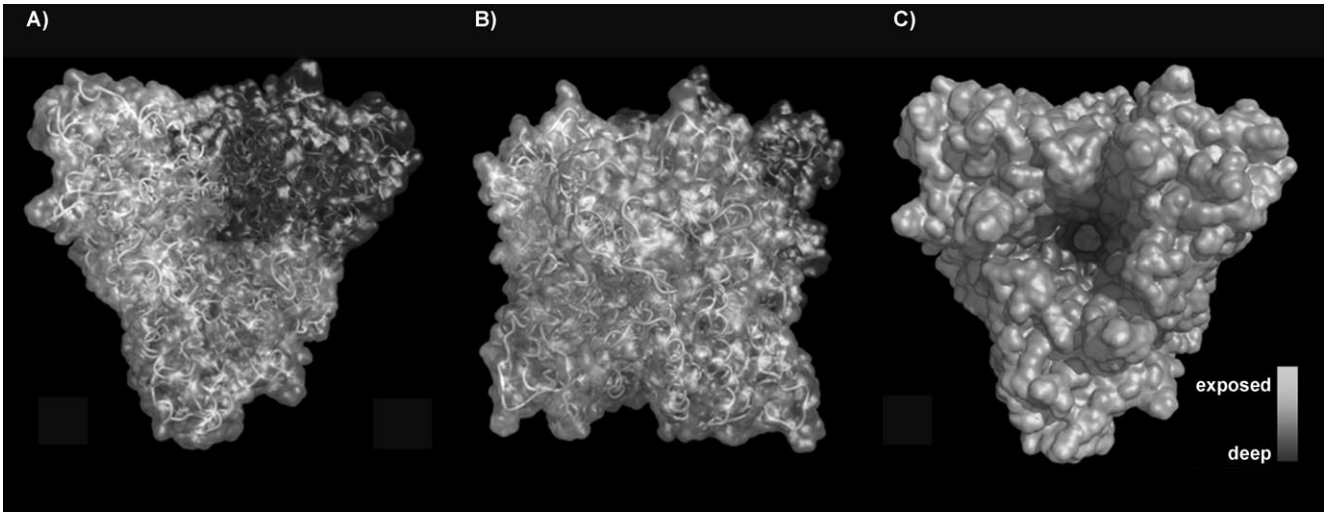

Figure 4. Tube structure of the EAAT1 homotrimeric model: A) homotrimeric model, colored by monomer, viewed from the extracellular side of the membrane; B) homotrimeric model, viewed parallel to the membrane; C) Solid surface of EAAT1 homotrimeric model viewed from the extracellular side of the membrane and coloured according its depth.

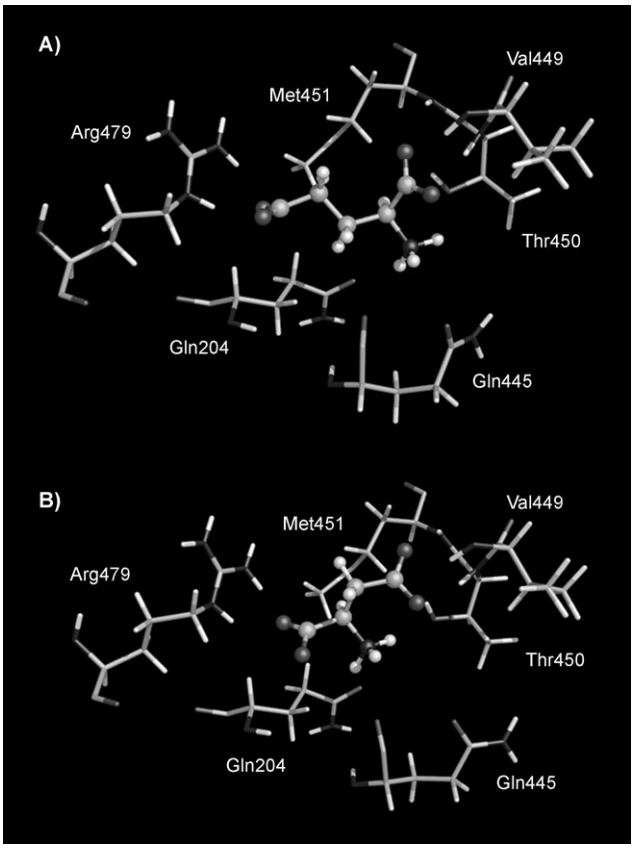

Figure 5. Main interactions stabilizing the complexes between natural substrates (A, L-glutamate and B, D-aspartate) and EAAT1.

Table 1. Activity values and docking results for transported compounds (**1**–**16**).

compd.	Activity [K_m, μM]	FlexScore [Kcal mol^{-1}]	d_{c-c} [Å]	Overlap Volume [Å^3]
1 (L-Glu)	20	−31.57	4.6	0.135
2 (L-Asp)	16	−38.49	4.0	0.022
3 (D-Asp)	23	−28.08	3.8	0.091
4 (2S4R4 MG)	54	−37.12	4.4	0.435
5 (2S4S4 MG)	Inactive	−26.87	4.5	0.745
6 (L-THA)	11	−32.09	4.6	0.061
7 (LT4HG)	61	−28.62	4.5	0.391
8 (L-SOS)	39	−17.02	5.1[a]	0.322
9 (LCCG-III)	13	−26.78	4.5	0.056
10 (DCCG-I)	50	−31.30	4.5	0.322
11 (L-CCG-IV)	278	−24.64	4.4	0.924
12 (t-2,4PDC)	28	−23.13	4.6	0.191
13 (2,4 MPDC)	87	−42.44	4.7	0.624
14 (3,4 MPDC)	37	−40.26	4.9	0.256
15 (4Me, 2,4-PDC)	43	−34.02	4.6	0.367
16 (cis-ACBD)	170	−24.33	4.6	0.576

fact that the interactions often involve the protein backbone instead of the side chains.

The binding site adaptability can also explain the fact that both aspartate isomers are transported by EAAT1. In particular, the binding mode of L-aspartate (**2**) is very similar to that of L-glutamate in its folded geometry, whereas D-aspartate (**3**, as reported in Figure 5B) unveils a reverse binding mode in which the ligand α-carboxylate interacts with Arg479 and the β-carboxylate with Val449, Thr450. The lower activity of D-aspartate may be due to fact that in such a reserve binding mode the β-carboxylate bumps somewhat against the Met451 side chain.

Taken together, these docking results afford a preliminary validation of EAAT1 binding site, revealing a set of polar interactions in excellent agreement with those observed in a recently resolved structure of the glutamate transporter homologue co-crystallized with aspartate.[33] Furthermore, these results disclose two quite contrasting features of the EAAT1 binding site: 1) the adaptability of the portion interacting with distal carboxylate, and 2) the global narrowness of the binding site which renders the steric factors of critical relevance for ligand bioactivity.

Docking results: Substrate inhibitors

The docking results, obtained by natural substrates, find interesting validations when analyzing the complexes for substrate inhibitors (**4**–**16**, Figure 1). For example, the docking analyses for 4-methyl glutamate isomers (**4**–**5**) provide compelling evidence for the key role of steric hindrance. Indeed, both isomers are able to realize the same set of polar interactions as seen in L-glutamate, but the steric hindrance elicited by methyl group induces a significant decrease of activity in the 2*S*, 4*R* isomer (**4**, as seen in Figure 6A) and is totally detrimental in 2*S*, 4*S* isomer (**5**), where the methyl group bumps against the side chains of Pro202 (TM4) distorting the fine architecture of the binding site.

Even avoiding a systematic description of docking results, the analysis of conformationally constrained cyclic analogues (**9**–**16**) can elucidate the bioactive conformation of EAAT1 ligands. For example, Figure 6B shows that the most active carboxycyclopropylglicine derivative (**9**, LCCG-III) interacts with EAAT1 assuming an intermediate geometry where the corresponding χ_1 torsion assumes an antiperiplanal geometry, while the corresponding χ_2 torsion is constrained in a planar conformation by cyclopropyl ring, resulting in a distance between the carboxylates equal to 4.3 Å. The most active pyrrolidine dicarboxylate derivative (**12**, L-trans-2,4-PDC) assumes a more extended conformation, as evidenced by the distance between carboxylates equal to 4.6 Å, and realizes the typical set of polar contacts as seen in L-glutamate even if the interactions involving the intra-anular ammonium group appear weakened (especially with Gln445) probably because of its limited accessibility (complex not shown).

Taken together, the docking results of substrate ligands unveil a set of polar interactions which involve all three ligand charged groups and which appear mandatory to induce the

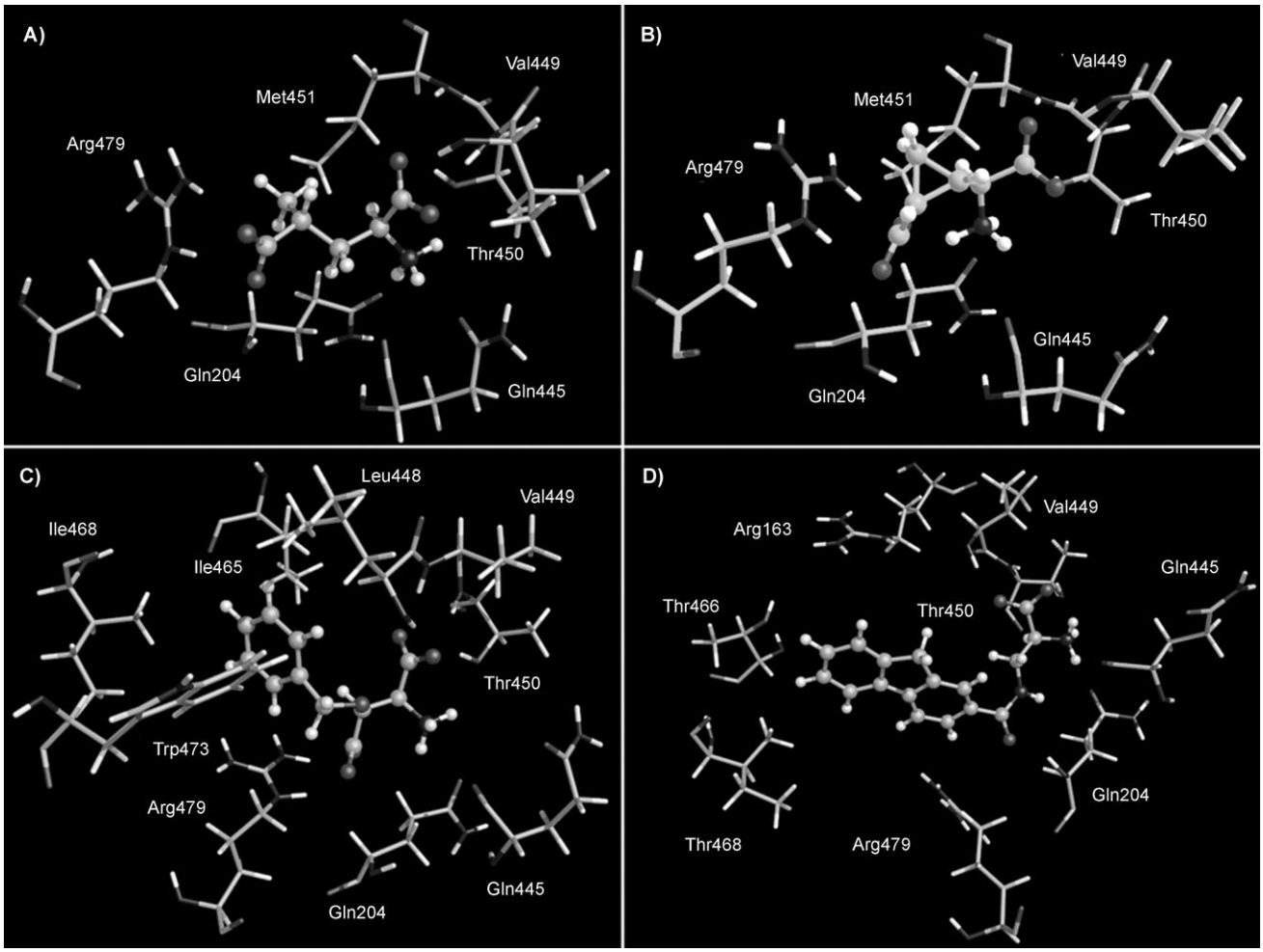

Figure 6. Main interactions stabilizing the complexes between EAAT1 and A) (2*S*, 4*R*)-4-Methylglutamate, B) L-CCGIII, C) L-TBOA, and D) fluorene DAPA derivative (32).

EAAT1 transport. The substrate inhibitors confirm the pivotal role of steric hindrance emphasizing the presence of two apolar regions with different steric requirements. The first, lined by Met 451, can accommodate small apolar groups with a modest decrease of bioactivity, whereas the latter, lined by Pro 202, cannot tolerate any moiety without losing bioactivity.

Table 1 reports the FlexScore for each substrate inhibitor, the distance between carboxylates, and the maximum overlapping between ligand and transporter (as computed by FlexX program). The distances between carboxylates confirm that EAAT1 can accept a broad assortment of ligand conformers as this distance can vary from 3.8 to 4.9 Å and this finding is in line with previous analyses.[14] The irrelevant correlation between bioactivity and docking scores ($r^2 \cong 0.10$) can be explained considering that the polar interactions are invariably present in all examined complexes and the steric clashes are not properly accounted by docking scores. Conversely, Equation 1 shows that ligand activities are linearly correlated with maximum overlapping volumes (V_{over}) which quantitatively describe the ligand ability to precisely fit into the binding site, providing a useful descriptor to predict the bioactivity of novel compounds.

$$\begin{aligned} &p K_m = 4.88(\pm 0.04) - 1.52(\pm 0.12)\, V_{over} \\ &n = 15,\ r^2 = 0.93,\ s = 0.11,\ F = 174.11 \end{aligned} \quad (1)$$

Even considering that the lack of protein flexibility in docking calculations can overestimate the extent of steric clashes, this relationship emphasizes the crucial role of steric factors in determining the ligand activity and suggests the opportunity to exploit geometric descriptors extracted by docking calculations instead of the usual docking scores to predict and rationalize ligand activity, especially when the precise fitting between ligand and biological target is even more important than the stabilizing contacts.

Docking results: Nontransported blockers

The analysis of docking results for the uptake blockers (Figure 2) begins with L-TMOA (**17**, complex not shown), which represents an inbetween derivative as it conserves a reduced electrogenicity (if compared to L-THA), realizing some interactions typical of blockers (as later described in this paragraph). Indeed, L-TMOA realizes the same polar interactions of L-THA

and inserts the methyl group in an apolar crevice lined by Leu448 (HP2), Ile465 (TM8), and Trp473 (TM8).

Figure 6C shows that L-TBOA (**18**), a prototypical example of EAAT1 blockers, inserts the phenyl ring in the aforementioned apolar cavity contacting several hydrophobic residues (for example, Leu448, Ile465, Ile468, and Trp473). The interaction of β-hydroxyaspartate derivatives with EAAT1 possesses a significant stereoselectivity: indeed, the poor activity of L-EBOA (**19**) and D-TBOA (**20**) is understandable considering their incapacity to correctly accommodate the phenyl ring in the described apolar cavity, even conserving many polar contacts.

The beneficial role of enlarged aromatic moieties is further confirmed when analyzing the results for phenylamidophenyloxy analogues. Thus, the most active derivative, TFB-TBOA (**26**), successfully inserts the aromatic system in the apolar cavity and the second phenyl ring is accommodated in the upper region of this crevice contacting many other hydrophobic residues [for example, Ile413 (HP2), Ala414 (HP2), and Leu467(TM8)]. The amidic function plays a dual role: 1) to assure a substantial planarity between the phenyl rings and 2) to take part in the EAAT1 interaction contacting Arg479.

The aspartic acid amides and the diaminopropionic acid analogues show an interaction pattern quite similar to that of β-hydroxyaspartate derivatives. Indeed, the amidic function interacts with Arg479 and the aromatic system is inserted in the aforementioned apolar cavity. Figure 6D shows the main interactions realized by the most active diaminopropionic acid derivative (**32**) in which the fluorene moiety assures the aromatic planarity, whose relevance was already observed in the previous compounds. The positive role of such planarity is easily explainable considering the narrowness of the apolar crevice which can successfully accommodate the enlarged aromatic system, whereas the aliphatic groups have difficultly to penetrate the cavity as demonstrated by the modest activity of the Piv-ATBOA analogue (**23**).

Interestingly, the distal ring in the fluorene moiety contacts a second arginine residue (Arg163 in EL2, as seen in Figure 6D) which further stabilizes the complex. When comparing the docking results for β-hydroxyaspartate amidic derivatives (**24**–**26**) with those for aspartamides and diaminopropionic acid analogues (**27**–**32**), one can note that whereas the first ones insert the distal aromatic ring in an upper region where the ligand can contact apolar residues only, in the last ones the distal ring is arranged in a more lateral region of such crevice where they can interact also with polar residues (for example Arg163 and Thr466 in TM8). Such a difference has a clear implication in the role of substituents, indeed, in the L-TBOA derivatives the substituents do not add extra interactions but maximize the local lipophilicity, whereas in aspartamides and diaminopropionic acid analogues such substituents can interact with the mentioned polar residues improving the ligand bioactivity.

Overall, the docking results for EAAT1 blockers emphasize the key role of an extended apolar cavity in which one can recognize three different pockets: 1) a lower region, lined by hydrophobic residues only, which connects the apolar cavity with the substrate binding site and with which all considered blockers interact; 2) a more lateral region, lined by hydrophobic and polar residues, with which aspartamides and diaminopropionic acid analogues only can interact (**27**–**32**), and 3) an upper region, lined by apolar residues only, with which amidic L-TBOA analogues only can interact (**23**–**26**).

Equation 2 illustrates the significant correlation between bioactivity of EAAT1 blockers and the FlexX scores (as compiled in Table 2). Interestingly, whereas the score values for EAAT1 substrates did not afford significant relations and the activity values were successfully related to overlap volumes, here the overlap volumes do not produce significant relationships and the FlexX scores do it. This suggests that the interactions realized by the aromatic system (that is, hydrophobic contacts and, especially, charge-transfer interactions), play a crucial role in determining the activity of EAAT1 blockers, whereas the insignificant role of steric hindrance can be explained as all blockers occupy the polar binding site with a very similar moiety (a derivative of aspartic acid). This also suggests that, whereas the polar binding site has a very limited volume, the

Table 2. Activity values, docking results, and pharmacophore predictions for nontransported blockers.

compd.	Activity [IC_{50}, μM]	FlexScore [Kcal mol^{-1}]	Estimated IC_{50} [μM] by docking	Overlap Volume [Å^3]	Estimated IC_{50} [μM] by HypoGen
L-TMOA (17)	69	−21.55	33	0.847	79
L-TBOA (18)	33	−32.80	8.3	0.343	48
D-TBOA (19)	637	−21.50	33	0.636	31
L-EBOA (20)	817	−25.06	11	0.594	170
TNOA1 (21)	15	−36.21	2.7	0.44	6.2
TNOA2 (22)	16	−30.96	15	0.594	9.3
PIVA-TBOA (23)	44	−34.88	4.2	0.599	9.3
CNB-TBOA (24)	0.286	−45.87	0.12	0.263	0.012
PMB-TBOA (25)	0.116	−47.04	0.081	0.369	0.011
TFB-TBOA (26)	0.022	−47.73	0.063	0.168	0.011
WAY-213613 (27)	5	−30.91	15	0.682	5.6
WAY-213394 (28)	1.97	−31.77	11	1.072	0.18
WAY-212922 (29)	3.4	−33.12	7.4	0.344	1
WAY-209429 (30)	1.03	−35.78	3.1	0.457	12
WAY-211686 (31)	1.7	−33.17	7.3	0.636	6.4
(32)	0.3	−37.65	1.7	0.857	8.3

apolar crevice has an enlarged volume which can accommodate a broad variety of aromatic systems.

$$pIC_{50} = 0.4446(\pm 0.07) - 0.141\ (\pm 0.02)\ \text{ScoreFlexX}$$
$$n = 16,\ r^2 = 0.77,\ s = 0.55,\ F = 43.46 \qquad (2)$$

Pharmacophore mapping

The ligand dataset was also used to generate two pharmacophore models, the first for EAAT1 substrates and the latter for EAAT1 blockers, defining the key features required for an optimal bioactivity. As the activity range of substrates is markedly smaller than that of blockers, pharmacophores were derived using two different approaches. For substrates we exploited the CATALYST/HipHop-Refine module (Catalyst, version 4.10, Accelrys Inc., San Diego, CA, 2006) which involves a qualitative description of pharmacophore hypotheses, while for blockers the CATALYST/Hypo-Refine algorithm gave a quantitative picture of derived models allowing a precise prediction of ligand bioactivities.

A training set consisting of eight structurally different substrates (**1**, **2**, **5**, **6**, **9**, **11**, **12**, and **16**) was submitted for pharmacophore building. Ten hypotheses were obtained with a ranking scores ranging from 84.9531 to 81.5959 (as compiled in Table S4 A, Supporting Information). Although the scores of the top four models were the same, the disposition of features and the number of excluded volumes were different from each other. Particularly, considering that the third ranking pharmacophore model (Figure 7 A) showed the best results in the validation tests, it was chosen as the model for this study. This contained one positive ionisable feature (P), four hydrogen bond acceptors (A1–A4) and nine excluded volumes (E1–E9). In an attempt to assess our developed pharmacophore model against the docking results, all substrates (**1**–**16**) in their bound conformation (as obtained by docking analyses) were mapped onto the pharmacophore hypothesis. The selected poses were able to overlap the model with fit values in line with the bioactivities, confirming the plausibility of the suggested binding modes.

As an example of a natural substrate, Figure 7 B shows the docking results of L-glutamate (**1**), mapped onto putative pharmacophore, showing that the docking result successfully over-

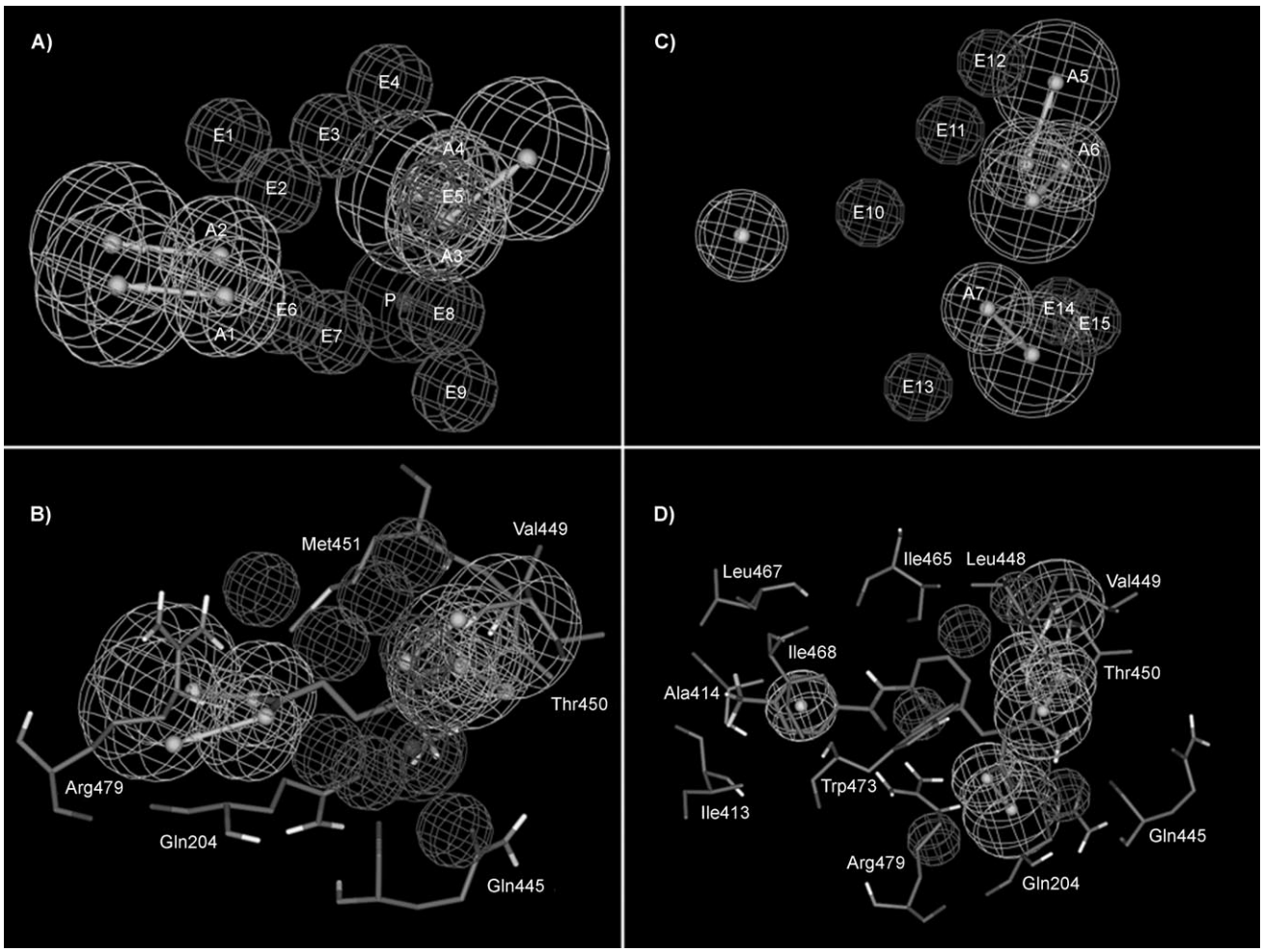

Figure 7. Pharmacophore models for EAAT1 ligands A) Pharmacophore features for EAAT1 natural and substrate inhibitors by Hip-Hop approach; B) Pharmacophore mapped on docking pose of L-Glutamate; C) Pharmacophore features for EAAT1 blockers by HypoRefine approach; D) Pharmacophore mapped on docking pose of TFB-TBOA.

lays all the pharmacophore features. More in detail, the α-carboxylate group of compound is able to occupy the hydrogen bond acceptor spheres (A1–A2) while γ-carboxylate maps the other two hydrogen bond acceptor features (A3–A4). Finally the positive ionisable feature (P) matches the ammonium group. These interactions confirmed the results obtained from docking studies: A1 and A2 overlap on the position of Arg 479; whereas A3 and A4 with those of Val 449 and Met 451; P occupies the positions of Gln 204, Gln 445, and Thr 450. The excluded volumes represent the position of other amino acids not involved in ligand interaction but able to create steric clashes with the less active compounds (for example, Met 451).

HypoRefine was exploited to derive an automated SAR pharmacophore model for nontrasported blockers using a training set of ten compounds (that is, **17**, **19**, **20**, **21**, **23**, **25**, **26**, **27**, **30**, and **32**) with a range of bioactivity, expressed as IC_{50}, spanning six orders of magnitude (0.022 μM to 817 μM) which makes this a suitable dataset for the HypoRefine approach. The ten hypotheses that showed the best correlation between estimated and measured activities, are compiled in Table S4 B (Supporting Information) as well as the results of statistical significance and predictive ability. The quality of the generated pharmacophore hypotheses was evaluated by considering the cost functions calculated by the HypoGen module during hypothesis generation.

The top ranked pharmacophore model (Hypo1) had the best predictive power and statistical significance and was characterized by the highest cost difference (98.402), the lowest RMS (0.91), and the best correlation coefficient (0.98). These values indicated the great predictability of the 3D-QSAR pharmacophore and confirmed that it did not come about by chance: Hypo1 was thus retained for further analysis (Table S4 B, Supporting Information). The selected 3 D hypothesis consisted of one hydrophobic region (Y), three hydrogen-bond acceptors (A5–A7), and six excluded volume sites (E10–E15) in a specific three-dimensional orientation (as seen in Figure 7 C).

Also in this case, to assess such quantitative pharmacophore model against the docking results, all blockers (**17**–**32**), in their bound conformation, were mapped onto the hypothesis and the activity were successfully predicted, confirming the soundness of the suggested binding modes.

Furthermore, the pharmacophore model accurately estimated the IC_{50} value of the bound conformation for the most active compound in the series. For example, the bound conformation of TFB-TBOA (**26**) overlays all the four pharmacophore features of the model (Figure 7 D). In detail, besides the interactions of the polar groups, this compound has a second phenyl ring which is able to properly map the Y feature of the generated hypothesis, thus confirming the positive influence of a lipophilic group on the biological activity of such class of nontransported blockers.

Finally, Table 2 reports the activity predicted by the pharmacophore model for all blockers (as obtained for bound conformations), revealing a satisfactory correlation ($r^2 = 0.60$) with the experimental bioactivities even if the model fails to both discriminate between the TBOA isomers and precisely predict the DAPAs (**31**–**32**) activities. The fact that docking results and pharmacophore predictions similarly correlate with bioactivities can be seen as a mutual validation of the respective algorithms used to calculate them and, globally, a reinforced validation of derived EAAT1 model.

Conclusions

The homogeneity of docking complexes, the agreement with mutational analyses, the consistency with pharmacophore hypotheses, and the relevant correlations between docking scores, pharmacophore fitting, and biological activities confirm the reliability of the EAAT1 model proposed herein. Taken globally, the obtained results allow to clearly discriminate between substrates, for which the precise fitting with the binding site seems to be of crucial relevance, and the blockers are characterized by extensive apolar contacts which enlarged aromatic moieties in a suitable hydrophobic pocket. Hopefully, such results will allow the rational design of improved EAAT1 ligands by both minimizing the steric hindrance of novel substrates and maximizing the apolar contacts of novel blockers.

Furthermore, this work emphasizes the fertile opportunity to exploit the resolved prokaryotic transmembrane proteins to model the corresponding eukaryotic structures. Indeed, the number of experimentally resolved prokaryotic transmembrane proteins has grown remarkably in the last years, more than that of eukaryotic ones.[34] Fortunately, about half of the eukaryotic transmembrane protein families have bacterial or archaeal homologues. This means that in many cases the folding of human transmembrane proteins can be predicted using the corresponding prokaryotic structures as templates. However, the homology approaches based on a unique template are not always the best choice as 1) some segments of eukaryotic proteins can be missing in the prokaryotic homologue (as seen in TM4 segment of EAAT1) and, thus, are unpredictable with the bacterial template; 2) a rigid use of a unique template can lead to a quite inaccurate model which does not account for the local peculiarities of the eukaryotic structures.

Considering these premises, the reliability of the described EAAT1 model emphasizes that the fragmental approach can successfully overcome the mentioned pitfalls of global homology becoming a versatile tool to generate improved full-length models which takes local features into account, even assuring a global agreement with the prokaryotic template. Intriguingly, the fragmental approach, which was first developed to overcome the drawbacks of rhodopsin-based methods in GPCR modelling, can find fertile applications in folding prediction of totally different transmembrane proteins.

Computational details

Generation of EAAT1 monomer

The amino acidic sequence of the human EAAT1 monomer was retrieved from Swiss-Prot database (entry code P43003, EAAT1_HUMAN). Despite the marked homology between human EAAT1 and glutamate transporter homologue from *Pyrococcus horikoshii* (64.6 %), there are three EAAT1 segments

which are unpredictable using the glutamate transporter homologue as the template. In particular, these gaps involve the two terminal domains (namely, 1–49 and 499–542), and the long loop in TM4 (namely, L4bc, 190–244). Therefore, the EAAT1 starting model was generated using a fragmental strategy which involves: 1) the fragmentation of amino acid sequence in 27 segments (namely 13 TM segments, 12 loops, and 2 terminal segments, as compiled in Table S3, Supporting Information), 2) the homology modeling of these segments separately, and 3) the assembly of fragments using the structure of glutamate transporter homologue (PDB Id: 1xfh) as a template.

The 27 segments were singly predicted using Fugue approach, an on-line 3D structure prediction software which generates realistic models recognizing distant homologies by sequence-structure comparison.[35] For each segment Fugue is able to produce several realistic models and the best structure has been chosen considering what result better fulfilled the following major conditions: 1) the predicted secondary structure from the sequence alignment using ClustalX[36] (data not reported); 2) the lack of not predicted gaps; 3) the prediction score (*ZSCORE*) as calculated by the Fugue program; 4) the helix conformation of eight transmembrane segments (TM1–TM8) with characteristic slight bending of the helices containing proline and glycine residues; 5) the multiple elements of TM4 having a corkscrew-like helix-turn-helix-turn-helix structure (namely, TM4a, L4ab, TM4b, L4bc, and TM4c); 6) the unusual folding of TM7 being formed by two parallel helical segments linked by a loop motif (TM7a, L7ab, and TM7b); 7) the helical hairpin folding for two transmembrane domains (HP1 and HP2); 8) the global "U" shape for the loops in which the two ends are close enough to join to TM segments.

Table S3 reports the templates used by Fugue to generate the best model for each fragment. Interestingly, 11 out of 27 segments were predicted using the glutamate transporter homologue as the template also with the fragmental approach, suggesting that these segments have an unusual folding which cannot be found in other proteins. In particular, the segments predicted by glutamate transporter homologue include: 1) the large transmembrane helices (namely, TM2, TM3, TM5, and TM8) which are, indeed, markedly longer than those of GPCRs, 2) the loops connecting these large helices (namely, EL1, CL1, EL2, CL2, EL3, and EL5), which show some particular features (for example, EL2 shows an extended arch-shape folding and EL3 has a proline-rich motif), and 3) the composite TM7 segment which has an unusual transmembrane folding. The helical hairpins are predicted in their helix-turn-helix structure using different templates depending on some local features (for example, the turn of HP1 presents a conserved serine-rich motif, wheras the tip of HP2 shows some conserved proline residues interacting with HP1).

Finally, the assembly of predicted fragments was performed superimposing the backbone of a fragment with that of the correspondent segment in the structure of the glutamate transporter homologue and manually connecting the adjacent segments using VEGA software.[37] In particular, the superimposition involved the Cα atoms of transmembrane helices only, as the loop arrangements, which were, however, defined considering the corresponding segment of experimental template, are clearly defined by the position of TMs, and their conformation was further relaxed by subsequent MD simulations (while the transmembrane bundle remains constrained during the molecular dynamics, as described in the next section).

Rotamer libraries were applied to insert side chains and hydrogen atoms were added using VEGA. According to physiological pH, Arg, Lys, Glu, and Asp residues were preserved ionized, whereas His residues were considered neutral by default. After a careful scrutiny of the obtained structure to avoid unphysical conditions, the EAAT1 monomer underwent an initial minimization until the RMS gradient was equal to one to discard high-energy interactions, followed by a local minimization until RMS = 0.05, where all atoms were kept fixed except for atoms included within a 5.0 Å sphere around the manually connected bonds (at the fragment ends). Finally, the model was optimized by a final minimization made up by two phases: first a minimization without constraints until RMS = 0.1 kcal mol^{-1} $Å^{-1}$ and then a second minimization with backbone fixed until RMS = 0.01 kcal mol^{-1} $Å^{-1}$ to preserve the predicted structure. In these phases and in the following steps the model goodness was assessed using Procheck[38] and Verify3D.[39]

To gain a better relaxation and a more correct arrangement of the whole EAAT1 monomer, a molecular dynamics equilibration was performed in vacuo. The simulations were carried out in three phases: 1) heating from 0 K to 300 K over 3000 iterations (3 ps, that is, 1 K/10 iterations), 2) starting equilibration of 2500 ps, where the transmembrane backbone was kept fixed, and 3) equilibration of 7500 ps, in which the transmembrane backbone was harmonically restrained with decreasing harmonic force constants. In more detail, harmonic force constant value was equal to 1 (1000 kJ mol^{-1} nm^{-2}) at the beginning of simulation and then was divided into two every 1.5 ns (then 5 MD were performed with harmonic force constant equal to 1, 0.5, 0.25, 0.12, and 0.06). Globally, the MD simulations lasted 10 ns and helices were correctly preserved with a harmonic force constant equal to 0.06. The last frame was used for the trimer assembly after a final minimization until rms = 0.01 (with harmonic force constant equal to 0.06).

The MD simulations had the following general characteristics: constant temperature at 300 ± 10 K by means of Langevin's algorithm; Lennard-Jones (L-J) interactions were calculated with a cut-off of 10 Å and the pair list was updated every 20 iterations; Newton's equation was integrated, using r-RESPA method, every 4 fs for long-range electrostatic forces, 2 fs for short-range non bonded forces, and 1 fs for bonded forces; a frame was stored every 5 ps, yielding 2000 frames. All calculations were carried out on a dual Athlon PC. All minimizations were performed using the conjugated gradients algorithm. The package Namd 2.51[40] was used with the force-field CHARMm v22 and Gasteiger's atomic charges.

Trimer assembly

As human EAAT1 possesses a homotrimeric quaternary structure, the obtained EAAT1 monomer was used to build the corresponding homotrimer through automatic docking using EscherNG program.[41] The trimer assembly is organized in two sequential steps. In the first step, two EAAT1 monomers are docked to obtain the corresponding homodimer and in the second step the dimer was docked with a third monomer to generate the final EAAT1 homotrimer. In detail, the z axis corresponds to the transmembrane direction, the thickness of the molecular slices was equal to 1.5 Å, the polygons were rotated with a step size of 20°, and 1000 possible solutions were produced. In both analyses, the best solution was selected considering: 1) the score of EscherNG, 2) the similarity with homotrimeric architecture of glutamate transporter homologue from *Pyrococcus horikoshii*, and 3) the accessibility of regions, which constitute the solvent accessible extracellular basin extending halfway across the membrane segment.

The obtained homotrimer underwent a preliminary minimization followed by a 1 ns MD simulation in a vacuum with transmembrane segments harmonically restrained with force constant equal to 0.06 and general characteristics equal to those described in the previous section. The last frame was used for the docking calculations after a final minimization until RMS = 0.01 kcal mol^{-1} Å^{-1} (with harmonic force constant equal to 0.06).

The shape of trimer assembly was analyzed using the DEEP surface as computed by VEGA software which allows cavities and protrusions in protein structures to be unveiled. In particular, the deepness of each point in the DEEP surface is derived by calculating the distance between the center of mass of the protein and the point itself. Then, this property is graphically represented coloring the points with a defined color ramp: blue denotes deep regions (that is, surface points with small distances from the barycenter) and green for exposed regions (that is, surface points with large distances from the barycenter).

Ligand datasets

Two sets of EAAT1 ligands were compiled from literature data. Figure 1 comprises EAAT1 transported ligands including both natural substrates (**1**–**3**) and competitive substrate inhibitors (**4**–**16**), activities of which were measured as K_m (μM) by two-electrode voltage clamp in cells expressing EAAT1 (as compiled in Table 1). In particular, this set includes the L-glutamate[42] (**1**) and both enantiomers of aspartate[43] (**2, 3**) as natural substrates. As substrate inhibitors the set includes: 4-methylglutamate isomers (**4**–**5**),[42] L-*threo*-β-hydroxyaspartate (THA, **6**),[6] L-*threo*-4-hydroxyglutamate (**7**),[42] L-sulphate-O-serine (L-SOS, **8**),[9] three cyclopropyl derivatives (namely, L-CCG-III, **9**, D-CCG-I, **10**, and L-CCG-IV, **11**),[44] four pyrrolidine dicarboxylates (namely, t-2,4 PDC, **12**, 2,4MPDC, **13**, L-3,4MPDC, **14**, 4-Methyl-2,4 PDC, **15**),[42] and cis-aminocyclobutyl dicarboxylate (cis-ABCD, **16**).[9] Figure 2 includes the nontransported blockers which can be divided in three main groups: β-hydroxyaspartate derivatives (**17**–**26**),[45,46] aspartic acid amides (**27**–**30**),[47] and diaminopropionic acid analogues (DAPAs, **31-32**).[48] The biological activities were measured as IC_{50} (μM) by the inhibition of L-glutamate uptake in cells transiently expressing EAAT1 (as compiled in Table 2).

All ligands were built preserving the reported stereochemistry (as indicated in Figures 1–2). The compounds were simulated in their ionized form as it is involved in transporter recognition. After a preliminary energy minimization to discard high-energy intramolecular interactions, the overall geometry and the atomic charges were optimized using *MOPAC6.0* (keywords: "AM1", "PRECISE", "GEO-OK", "MMOK").

Docking analyses

The FlexX program was used to dock all considered compounds to the EAAT1 binding sites. FlexX is a fast-automated docking program that considers ligand conformational flexibility by an incremental fragment placing technique.[49] In this study, the docking analysis involved the EAAT1 monomer, as extracted from the optimized homotrimer model. The docking searchers were focused on residues enclosed within 15.0 Å radius sphere centered on Arg 479 (TM4) so that the ligands should interact with all residues recognized by mutational analyses. For each molecule, 30 docking solutions (poses) were computed and scored. The best complexes were chosen considering the best score docking result in which at least a ligand's carboxylate interacts with Arg 479.

Pharmacophore generation

All structures were generated using the 2D/3D editor sketcher in the Catalyst 4.10 software package (Catalyst, version 4.10; Accelrys Inc., San Diego, CA, 2006) and submitted to energy minimization and conformational analysis (maximum number of conformers = 250, generation type: best quality, energy range = 10 kcal mol^{-1}).

Catalyst provides a dictionary of chemical features found to be important in drug–enzyme/receptor interactions. These are hydrogen bond donors, hydrogen bond acceptors, aromatic ring, hydrophobic (aliphatic or aromatic) groups, and positive and negative ionisable groups. The interfeature spacing penalty was reduced from its default value to 50 pm. No constraint on the minimum and maximum number of each type of feature in the reported pharmacophores was applied.

The pharmacophore model for substrates was generated by HipHop-Refine module[50] of Catalyst 4.10 using a training set of eight structurally different natural substrate and substrate inhibitors (**1**, **2**, **5**, **6**, **9**, **11**, **12**, and **16**). HipHop-Refine was configured as follows. Compounds of $K_m < 30$ μM (**1**, **2**, **6**, **9**, **12**) were considered "active" and were assigned values to Principal and MaxOmit Features of 2 and 0, respectively. Compounds of $K_m > 100$ μM (**11** and **16**) were considered "moderately active" and were assigned values to Principal and MaxOmitFeatures of 1. Compound **5** was reported to be inactive and therefore was assigned a Principal value of 0; furthermore, considering that its inactivity seems largely due to steric properties, a MaxOmit-

Features value was set to 0. On the basis of the atom types in the molecules of the training set, four chemical feature types were used in the HipHop-Refine run: hydrogen bond acceptor (HBA), hydrogen bond donor (HBD), hydrophobic (HY), positive ionisable (P).

The pharmacophore model for blockers was generated by HypoRefine module of Catalyst 4.9[51] using a training set of 10 EAAT1 blockers (that is, **17**, **19**, **20**, **21**, **23**, **25**, **26**, **27**, **30**, and **32**). Specifically, we selected compounds with different degree of activity, spanned six orders of magnitude, making this a good data set for HypoRefine module. The uncertainty value of compounds activity, which represents the ratio range of uncertainty in the activity value based on the expected statistical variability of biological data collection, was set to 2. In the development of 3D hypothesis by Catalyst HypoRefine, the difference in the steric bulk between the most active and the inactive compounds are labeled in the "principal" column of the input spreadsheet: for our study we chose **26** ($IC_{50}=0.022$ μM) as active compounds (labeled with digit 2) and the compound **20** ($IC_{50}=817$ μM) as inactive (labeled with digit 1) . On the basis of the atom types in the molecules of the training set, five chemical feature types were used in the HypoGen run: hydrogen bond acceptor (HBA), positive ionisable (P), hydrophobic (HY), hydrophobic aliphatic (HYAl), and hydrophobic aromatic (HYAr) groups.

Acknowledgements

Financial support for this research by Italian Ministry of Education, University, and Research (Grant FIRB2003) is gratefully acknowledged.

Keywords: EAAT1 blockers · EAAT1 · fragmental homology modeling · molecular docking · pharmacophore mapping

[1] H. Brauner-Osborne, J. Egebjerg, E. O. Nielsen, U. Madsen, P. Krogsgaard-Larsen, *J. Med. Chem.* **2000**, *43*, 2609–2645.
[2] J. N. Kew, J. A. Kemp, *Psychopharmacology* **2005**, *179*, 4–29.
[3] D. W. Choi, M. Maulucci-Gedde, A. R. Kriegstein, *J. Neurosci.* **1987**, *7*, 357—368.
[4] C. Matute, M. Domercq, M. V. Sanchez-Gomez, *Glia* **2006**, *53*, 212–224.
[5] N. C. Danbolt, *Prog. Neurobiol.* **2001**, *65*, 1—105.
[6] Y. Shigeri, R. P. Seal, K. Shimamoto, *Brain Res. Rev.* **2004**, *45*, 250–265.
[7] C. Grewer, T. Rauen, *J. Membr. Biol.* **2005**, *203*, 1–20.
[8] R. J. Bridges, C. S. Esslinger, *Pharmacol. Ther.* **2005**, *107*, 271–285.
[9] G. Campiani, C. Fattorusso, M. De Angelis, B. Catalanotti, S. Butini, R. Fattorusso, I. Fiorini, V. Nacci, E. Novellino, *Curr. Pharm. Des.* **2003**, *9*, 599–625.
[10] E. Hinoi, T. Takarada, Y. Tsuchihashi, Y. Yoneda, *Curr. Drug Targets: CNS Neurol. Disord.* **2005**, *4*, 211–220.
[11] J. Dunlop, J. A. Butera, *Curr. Top. Med. Chem.* **2006**, *6*, 1897–1906.
[12] C. M. Anderson, R. J. Bridges, A. R. Chamberlin, K. Shimamoto, Y. Yasuda-Kamatani, R. A. Swanson, *J. Neurochem.* **2001**, *79*, 1207–1216.
[13] D. J. Rossi, T. Oshima, D. Attwell, *Nature* **2000**, *403*, 316–321.
[14] T. Mennini, E. Fumagalli, M. Gobbi, C. Fattorusso, B. Catalanotti, G. Campiani, *Eur. J. Pharmacol.* **2003**, *479*, 291–296.
[15] G. Gegelashvili, A. Schousboe, *Brain Res. Bull.* **1998**, *45*, 233–238.
[16] T. Rauen, *Amino Acids* **2000**, *19*, 53–62.
[17] M. Bouvier, M. Szatkowski, A. Amato, D. Attwell, *Nature* **1992**, *360*, 471–474.
[18] U. V. Berger, M. A. Hediger, *Anat. Embryol.* **2006**, *211*, 595–606.
[19] M. P. Kavanaugh, *Nature* **2004**, *431*, 752–753.
[20] R. P. Seal, B. H. Leighton, S. G. Amara, *Neuron* **2000**, *25*, 695–706.
[21] A. D. Mitrovic, S. G Amara, G. A Johnston, R. J. Vandenberg, *J. Biol. Chem.* **1998**, *273*, 14698–14706.
[22] M. Conradt, W. Stoffel, *J. Biol. Chem.* **1995**, *270*, 25 207–25 212.
[23] R. P. Seal, S. G. Amara, *Neuron* **1998**, *21*, 1487–1498.
[24] R. P. Seal, Y. Shigeri, S. Eliasof, B. H. Leighton, S. G. Amara, *Proc. Natl. Acad. Sci. USA* **2001**, *98*, 15324–15329.
[25] D. Yernool, O. Boudker, Y. Jin, E. Gouaux, *Nature* **2004**, *431*, 811–818.
[26] B. H. Leighton, R. P. Seal, S. D. Watts, M. O. Skyba, S. G. Amara, *J. Biol. Chem.* **2006**, *281*, 29788–29796.
[27] K. Ginalski, N. V. Grishin, A. Godzik, L. Rychlewski, *Nucleic Acids Res.* **2005**, *33*, 1874–1891.
[28] A. Pedretti, M. Villa, M. Pallavicini, E. Valoti, G. Vistoli, *J. Med. Chem.* **2006**, *49*, 3077–3085.
[29] A. Pedretti, G. Vistoli, *Bioorg. Med. Chem.* **2007**, *15*, 3054–3064.
[30] D. J. Slotboom, I. Sobczak, W. N. Konings, J. S. Lolkema, *Proc. Natl. Acad. Sci. USA* **1999**, *96*, 14282–14287.
[31] M. Grunewald, D. Menaker, B. I. Kanner, *J. Biol. Chem.* **2002**, *277*, 26074–26080.
[32] D. J. Slotboom, W. N. Konings, J. S. Lolkema, *J. Biol. Chem.* **2001**, *276*, 10775–10781.
[33] O. Boudker, R. M. Ryan, D. Yernool, K. Shimamoto, E. Gouaux, *Nature* **2007**, *445*, 387–393.
[34] S. J. Fleishman, V. M. Unger, N. Ben-Tal, *Trends Biochem. Sci.* **2006**, *31*, 106–113.
[35] J. Shi, T. L. Blundell, K. Mizuguchi, *J. Mol. Biol.* **2001**, *310*, 243–257.
[36] J. D. Thompson, T. J. Gibson, F. Plewniak, F. Jeanmougin, D. G. Higgins, *Nucleic Acids Res.* **1997**, *25*, 4876–4882.
[37] A. Pedretti, L. Villa, G. Vistoli, *J. Mol. Graphics* **2002**, *21*, 47–49.
[38] R. A. Laskowski, M. W. MacArthur, D. S. Moss, J. M. Thornton, *J. Appl. Crystallogr.* **1993**, *26*, 283–291.
[39] J. U. Bowie, R. Luthy, D. Eisenberg, *Science* **1991**, *253*, 164–170.
[40] L. Kalé, R. Skeel, M. Bhandarkar, R. Brunner, A. Gursoy, N. Krawetz, J. Phillips, A. Shinozaki, K. Varadarajan, K. Schulten, *J. Comput. Phys.* **1999**, *151*, 283–312.
[41] L. De Luca, A. Pedretti, G. Vistoli, M. L. Barreca, L. Villa, P. Monforte, A. Chimirri, *Biochem. Biophys. Res. Commun.* **2003**, *310*, 1083–1088.
[42] R. J. Vandenberg, A. D. Mitrovic, M. Chebib, V. J. Balcar, G. A. Johnston, *Mol. Pharmacol.* **1997**, *51*, 809–815.
[43] J. L. Arriza, W. A. Fairman, J. I. Wadiche, G. H. Murdoch, M. P. Kavanaugh, S. G. Amara, *J. Neurosci.* **1994**, *14*, 5559–5569.
[44] C. Moussa, A. D. Mitrovic, R. J. Vandenberg, T. Provis, C. Rae, W. A. Bubb, V. J. Balcar, *Neurochem. Res.* **2002**, *27*, 27–35.
[45] K. Shimamoto, Y. Shigeri, Y. Yasuda-Kamatani, B. Lebrun, N. Yumoto, T. Nakajima, *Bioorg. Med. Chem. Lett.* **2000**, *10*, 2407–2410.
[46] K. Shimamoto, R. Sakai, K. Takaoka, N. Yumoto, T. Nakajima, S. G. Amara, Y. Shigeri, *Mol. Pharmacol.* **2004**, *65*, 1008–1015.
[47] J. Dunlop, H. B. McIlvain, T. A. Carrick, B. Jow. Q. Lu, D. Kowal, S. Lin, A. Greenfield, C. Grosanu, K. Fan, R. Petroski, J. Williams, A. Foster, J. Butera, *Mol. Pharmacol.* **2005**, *68*, 974–982.
[48] A. Greenfield, C. Grosanu, J. Dunlop, B. McIlvain, T. Carrick, B. Jow, Q. Lu, D. Kowal, J. Williams, J. Butera, *Bioorg. Med. Chem. Lett.* **2005**, *15*, 4985–4988.
[49] M. Rarey, B. Kramer, T. Lengauer, G. Klebe, *J. Mol. Biol.* **1996**, *261*, 470–489.
[50] D. Barnum, J. Greene, A. Smellie, P. Sprague, *J. Chem. Inf. Comput. Sci.* **1996**, *36*, 563–571.
[51] H. Li, J. Sutter, R. Hoffmann in *Pharmacophore Perception, Development, and Use in Drug Design*, International University Line, La Jolla, **2000**, pp. 172–189.

Received: August 3, 2007
Revised: September 21, 2007
Published online on November 7, 2007

